HHS Public Access

Author manuscript

Aerosol Sci Technol. Author manuscript; available in PMC 2023 December 06.

Published in final edited form as:

Aerosol Sci Technol. 2021 ; 55(2): 142–153. doi:10.1080/02786826.2020.1829536.

The influence of temperature, humidity, and simulated sunlight on the infectivity of SARS-CoV-2 in aerosols

Paul Dabisch[a], **Michael Schuit**[a], **Artemas Herzog**[b], **Katie Beck**[a], **Stewart Wood**[a], **Melissa Krause**[a], **David Miller**[a], **Wade Weaver**[a], **Denise Freeburger**[a], **Idris Hooper**[a], **Brian Green**[a], **Gregory Williams**[a], **Brian Holland**[a], **Jordan Bohannon**[a], **Victoria Wahl**[a], **Jason Yolitz**[a], **Michael Hevey**[a], **Shanna Ratnesar-Shumate**[a]

[a]National Biodefense Analysis and Countermeasures Center, Operated by BNBI for the U.S. Department of Homeland Security Science and Technology Directorate, Frederick, Maryland, USA

[b]Censeo Insight Inc, Seattle, Washington, USA

Abstract

Recent evidence suggests that respiratory aerosols may play a role in the spread of SARS-CoV-2 during the ongoing COVID-19 pandemic. Our laboratory has previously demonstrated that simulated sunlight inactivated SARS-CoV-2 in aerosols and on surfaces. In the present study, we extend these findings to include the persistence of SARS-CoV-2 in aerosols across a range of temperature, humidity, and simulated sunlight levels using an environmentally controlled rotating drum aerosol chamber. The results demonstrate that temperature, simulated sunlight, and humidity are all significant factors influencing the persistence of infectious SARS-CoV-2 in aerosols, but that simulated sunlight and temperature have a greater influence on decay than humidity across the range of conditions tested. The time needed for a 90% decrease in infectious virus ranged from 4.8 min at 40 °C, 20% relative humidity, and high intensity simulated sunlight representative of noon on a clear day on the summer solstice at 4°N latitude, to greater than two hours under conditions representative of those expected indoors or at night. These results suggest that the persistence of infectious SARS-CoV-2 in naturally occurring aerosols may be affected by environmental conditions, and that aerosolized virus could remain infectious for extended periods of time under some environmental conditions. The present study provides a comprehensive dataset on the influence of environmental parameters on the survival of SARS-CoV-2 in aerosols that can be utilized, along with data on viral shedding from infected individuals and the inhalational infectious dose, to inform future modeling and risk assessment efforts.

Introduction

Severe acute respiratory syndrome coronavirus 2 (SARS-CoV-2) is the causative microorganism of COVID-19, an acute respiratory disease characterized by fever, cough, fatigue, and shortness of breath (Docherty et al. 2020; Lovato and de Filippis 2020). While

Disclosure statement

The authors have no conflicts of interest to disclose.

the relative contributions of potential routes of transmission to the spread of COVID-19 during the ongoing pandemic remain uncertain, recent evidence suggests that respiratory aerosols may play a role. Specifically, SARS-CoV-2 RNA was present in particles with aerodynamic diameters less than 4 μm collected in clinical settings (Chia et al. 2020; Liu et al. 2020). Similarly, viral genetic material has been recovered from exhaust vent covers in patient rooms, suggesting the presence of airborne virus (Guo et al. 2020). In another study, coronavirus RNA was detected in particles with aerodynamic diameters less than 5 μm collected from the exhaled breath of individuals infected with the seasonal coronaviruses NL63, OC43, or HKU1, suggesting the possibility that SARS-CoV-2 may be shed from the respiratory tract during normal breathing (Leung et al. 2020).

The transmission of virus by aerosols is potentially influenced by many factors, including the concentration and particle size distribution of virus-laden particles shed by infected individuals, how long airborne virus remains infectious under different environmental conditions, the proximity of individuals and airflow characteristics in a given space, and the amount of virus needed to be inhaled to cause infection. Numerous studies have examined how long coronaviruses remain infectious in aerosols under different environmental conditions. Recent studies have demonstrated that SARS-CoV-2 is relatively stable in aerosols under conditions similar to those expected for climate-controlled indoor environments, with decay rates reported to be less than 3% per minute, or greater than 75 min for a 90% loss of infectious virus (Smither et al. 2020; van Doremalen et al. 2020; Fears et al. 2020; Schuit, Ratnesar-Shumate et al. 2020). Similarly, Ijaz et al. (1985) reported that coronavirus 229E was also stable under comparable conditions. In the presence of ultraviolet radiation similar to that present in natural sunlight, our laboratory has previously reported that the decay rate for SARS-CoV-2 significantly increased to 26.1 ± 7.1% per minute, or a loss of 90% of infectious virus approximately every 8 min (Schuit, Ratnesar-Shumate et al. 2020). Temperature has also been reported to be positively correlated with the decay rate of aerosolized coronavirus 229E and MERS coronavirus (Ijaz et al. 1985; Pyankov et al. 2018). However, no data have been reported for the effect of temperature on the decay rate of SARS-CoV-2 in aerosols. Humidity is known to affect the stability of coronaviruses in aerosols. The decay rate of coronavirus 229E was significantly greater at either 80% or 30% relative humidity compared to 50% relative humidity (Ijaz et al. 1985). A dependence on relative humidity has also been reported for SARS-CoV-2, although the magnitude of this effect was dependent on the suspension matrix (Smither et al. 2020).

In the present study, we extend the findings of our previous study to examine the decay of SARS-CoV-2 in aerosols across a wider range of environmental conditions. Specifically, we measured the decay rate of aerosolized SARS-CoV-2 across a range of temperatures (from 10 °C to 40 °C), relative humidity levels (20% to 70%), and simulated sunlight levels (darkness to 1.9 W/m^2 integrated UVB). The decay rate data were utilized to develop a regression model to allow prediction of the decay rate of SARS-CoV-2 infectivity at any combination of temperature, humidity, and sunlight intensity within the ranges evaluated. These data, in conjunction with data on the viral load shed by infected individuals and the inhalational infectious dose, will be useful to inform modeling to better understand the impact of environmental conditions on the risk associated with various transmission scenarios.

Materials and methods

Vero Cells (ATCC CCL-81) were grown as described previously (Ratnesar-Shumate et al. 2020; Schuit, Ratnesar-Shumate et al. 2020). An isolate of SARS-CoV-2 (Passage 4; BetaCoV/USA/WA1/2020) was obtained from BEI resources and passaged twice in Vero cells to produce a stock of virus that was concentrated by tangential flow filtration and frozen at −80 °C until use. For each day of aerosol tests, an aliquot of the concentrated virus was thawed and diluted 1:10 in simulated saliva, as described previously (Ratnesar-Shumate et al. 2020; Schuit, Ratnesar-Shumate et al. 2020). The solids content was measured using a MA35 Moisture Analyzer (Sartorius AG). Protein concentration of viral suspensions was measured using a Pierce BCA Protein Assay Kit (23225, Thermo Fisher Scientific) with a mucin standard curve read on a SpectraMax M5 plate reader (Molecular Devices). The concentration of infectious virus in both stock suspensions and aerosol samples was determined by microtitration assay on confluent monolayers of Vero cells in 96-well plates. Plates were incubated at 37 °C and 5% CO_2, with cytopathic effect read four days post-infection and viral titers calculated using the Spearman-Kärber method. Results are reported as the number of median tissue culture infectious doses ($TCID_{50}$) present per mL of sample.

A 16-L environmentally controlled rotating drum chamber, with an internal diameter of 10.5” and rotating at 7.5 rpm, was utilized in the present testing to assess the decay of aerosolized SARS-CoV-2 (Figure 1; Schuit, Gardner, et al. 2020). Air temperature, humidity, and simulated sunlight levels were all controlled during testing. The air temperature inside the chamber was controlled by adjusting the temperature of polypropylene glycol circulating through the walls of the chamber. The temperature was measured at three points within the chamber using two type K thermocouples located in the center of the chamber (Traceable Products) and one combination temperature/relative humidity probe located near the wall of the chamber (Vaisala). Temperatures measured at these points in the chamber were in close agreement for tests at 20 °C. However, a small temperature gradient (<5 °C) was observed between the probe located near the wall of the chamber and the probes located in the center of the chamber during tests at temperatures further from room temperature, due to temperature-controlled polypropylene glycol flowing through the walls of the chamber. The mean temperature for each test was calculated from the data collected by all three probes over the duration of the test. The humidity inside the chamber was controlled by varying the mix of dry and humid air used to supply the chamber during aerosol filling and sampling, and monitored using the combination temperature/relative humidity probe located near the wall of the chamber (Vaisala). To account for temperature gradients present in the chamber, the absolute humidity measured by the probe near the chamber wall was used to calculate the relative humidity present at the two temperature probes located in the center of the chamber, and the mean relative humidity for each test was calculated as the mean of values for the three probes over the duration of a given test. Simulated sunlight was introduced into the chamber through an 8” quartz glass window located on one end of the chamber (Figure 1). Simulated sunlight was generated using solar simulator (94,083 A, Newport). The stock reflecting mirror was replaced with a longpass dichroic mirror to minimize reflection of visible and infrared wavelengths. A 320-nm highpass filter (WG320 filter PN SL07614, Solar Light Co.) was used to shape the

reflected light before it entered the chamber. The irradiance in the chamber was controlled using a manual iris, installed just downstream of the 320-nm highpass filter. The spectra utilized were intended to match the UV portion of spectra predicted by the National Center for Atmospheric Research (NCAR) Tropospheric Ultraviolet and Visible (TUV) radiation model (NCAR 2020) at noon for different times of year at 40°N latitude. Spectra produced by the solar simulator were measured immediately outside of the chamber window using a spectroradiometer (OL756, Gooch & Housego) equipped with a 2-inch diameter integrating sphere light receptor (IS-270, Gooch & Housego), and corrected for transmission losses through the fusedsilica window. Simulated sunlight levels are expressed as the integrated UVB irradiance, as a previous study demonstrated that exposure of SARS-CoV-1 to UVA did not significantly decrease infectivity (Darnell et al. 2004). A representative spectrum, compared to a target spectrum from the NCAR TUV radiation model is shown in Figure 2 (Schuit, Ratnesar-Shumate et al. 2020). No irradiance above the background measured in darkness was present in the spectrum generated by the solar simulator below approximately 295 nm (Figure 2).

Previous studies have reported the presence of viral genetic material in respiratory particles less than 5 μm aerodynamic diameter (Leung et al. 2020; Lindsley et al. 2010; Yang, Elankumaran, and Marr 2011). Therefore, a target mass median aerodynamic diameter (MMAD) in this range, specifically 2 μm, was used in the present study. Aerosol was generated using an air assist nozzle (IAZA5200415K; Lee Company) supplied with 200 μl/min of viral suspension and 14.7 L/min (45 psig) of compressed air into a stainless steel plenum to allow equilibration prior to entry into the drum. In addition to the aerosol generator, 27.3 L/min of humidity-controlled dilution air was supplied to the stainless steel plenum, for a total flow of 42 L/min. The output of the plenum was directed through a HEPA filter for the first minute after the start of aerosol generation to allow the concentration to reach steady state. After one minute, the inlet valve to the rotating drum was opened, and 20 L/min of the plenum flow was diverted into the rotating drum for 20–30 s to fill the drum. This filling duration produced a measurable concentration of infectious virus while minimizing disruption of temperature and humidity levels in the drum as well as decay of viral infectivity during drum filling.

Following chamber loading, aerosol samples were collected periodically from sampling ports located on a non-rotating band on the wall of the chamber. Test durations ranged from 20 min with simulated sunlight present to 60 min in darkness. An Aerodynamic Particle Sizer (APS; Model 3321, TSI Inc.) was used to measure the mass concentration and size distribution of the aerosol present in the drum, and 25 mm gelatin filters (PN 225–9551; SKC, Inc.) in Delrin filter holders (PN 1109; Pall Corp.) were used to collect samples for measurement of infectious virus. The APS and gelatin filters both flowed at 5 L/min. Gelatin filter flows were controlled using a mass flow controller (Alicat Scientific). Five paired APS and filter samples were collected over the course of each test. For each pair of samples, a ten second APS sample (0.83 L total volume) was followed immediately by a 20 s filter sample (1.67 L total volume). Immediately following sample collection, filters were removed from their holders, placed in conical tubes containing 10 mL of viral growth medium to dissolve the filter and re-suspend collected virus (Schuit, Ratnesar-Shumate et al. 2020). The recovered viral suspensions were assayed for infectious virus via microtitration

assay as already described. Assay results were used to estimate the infectious aerosol concentration present at each sample time point and expressed as $\log_{10}$ $TCID_{50}$/L air.

Decreases in the infectious aerosol concentration over time measured with the gelatin filters can be due to loss of infectivity of virus contained within the particles or physical losses of aerosol particles within the chamber. Physical losses of aerosol particles within the chamber were estimated from the mass concentration data obtained with the APS. The slopes of the best fit lines for time-series $\log_{10}$-transformed infectious and mass aerosol concentrations from each test were used as estimates of the total and physical decays, respectively. The difference between the estimates of total and physical decay represents the decay of viral infectivity. Representative plots of total and physical decay are shown in Figure 3. Linear regression analyses were performed in Microsoft Excel (version 16.0.5005.1000). For consistency with a previous study reported by our laboratory, decay rates were converted from $\log_{10}$ to $\log_e$, which is equivalent to the decay constant, $k_{infectivity}$, reported in this previous study (Schuit, Gardner, et al. 2020). All values are reported as arithmetic mean and standard deviation unless otherwise noted.

Tests were conducted across a range of combinations of temperature, humidity, and simulated sunlight to assess the influence of each factor on the decay of aerosolized SARS-CoV-2, as well as to identify any interactions between the factors. Three different temperature levels were assessed: 10 °C, 20 °C, and 30 °C. At each tempeature level, the influence of relative humidity and simulated sunlight was assessed using a 2^2 factorial experimental design with a center point. The high and low levels of relative humidity were 20% and 70%. The high and low levels of simulated sunlight were zero integrated UVB irradiance, or darkness, and 1.9 W/m^2 integrated UVB irradiance, similar to the spectrum predicted by the NCAR TUV radiation model for a cloudless 21 June day at noon at sea level at 40°N latitude (Figure 2). The midpoint condition at each temperature was 45% relative humidity and 0.9 W/m^2 integrated UVB irradiance.

Stepwise weighted least squares multiple regression was utilized to assess which environmental parameters significantly affected the decay constant for viral infectivity ($k_{infectivity}$) using JMP (v.11.2.0, SAS Institute Inc.). A main effects model that included first order interactions and second order main effects was initially assumed. Stepwise regression was used to identify and remove predictors based on their contribution to the model's Akaike information criterion (AIC). Terms that did not significantly contribute to the AIC were removed using a backward elimination approach. Residual analysis on the resulting model fit found a significant amount of heteroskedasticity in the residuals that appeared to be a function of simulated sunlight level. To account for the heteroskedasticity, the data were weighted by the inverse of the variance for $k_{infectivity}$ pooled for each solar level. The mean relative humidity and temperature from each individual test were used in the model. Analyses were also performed using absolute humidity instead of relative humidity as several studies have suggested that absolute humidity is a predictor of viral inactivation and disease tranmission (Barreca and Shimshack 2012; McDevitt et al. 2010; Shaman, Goldstein, and Lipsitch 2011). Integrated UVB irradiance measured for the different levels of simulated sunlight prior to testing was used in the model as it was not possible to make this measurement during experiments. Environmental parameters were standardized to a

range spanning −1 to +1 to allow direct comparison of the parameter estimates from the regression model. A total of 66 tests were included in these analyses. A minimum of three replicate tests were conducted at each combination of temperature, humidity, and simulated sunlight tested. Several tests with poor regression fits of the time series viral concentration data, specifically r^2 values below 0.70 and RMSE of greater than 0.3 $\log_{10}$ $TCID_{50}$/L air, were not included in multiple regression analyses.

Additional tests were also conducted at a higher temperature of 40 °C, as this temperature is relevant to many parts of the United States during the summer months, at a single relative humidity of 20%, and either 0.0 W/m^2 and 1.9 W/m^2 integrated UVB. Four replicate tests were conducted at each simulated sunlight level. These data are presented, but were not included in the multiple regression analyses since it was not possible to perform tests at all combinations of conditions in the 2^2 + center point design due to limitations of the test system, specifically an inability to achieve 70% relative humidity at this temperature for reasons discussed previously (Schuit, Ratnesar-Shumate et al. 2020).

Results

Concentrated SARS-CoV-2 viral suspensions diluted in simulated saliva had a solids content of 1.32 ± 0.03% (n = 3), significantly greater than the 1.01 ± 0.10% (n = 16) measured for simulated saliva alone (P< 0.0001 when compared using an unpaired t-test). Similarly, the viral suspension diluted in simulated saliva had a greater protein concentration (3.58 ± 0.07 mg/mL, n = 3) than measured for simulated saliva alone (0.68 ± 0.00 mg/mL; n = 3; P< 0.0001 when compared using an unpaired t-test).

The infectious viral concentration measured on the first sample was consistent across all tests, with a mean value of 2.3 ± 0.4 $\log_{10}$ $TCID_{50}$/L-air (CV = 16.0%). The mass concentration measured on the first sample was also consistent across all tests, with a mean value of 1.5 ± 0.1 $\log_{10}$ μg/L-air (CV = 6.0%). The mean MMAD and geometric standard deviation (GSD) measured at the first sample for each test were 1.94 ± 0.05 μm and 1.63 ± 0.01, respectively (n = 74). A small but significant decrease in the MMAD and GSD was observed over the course of a test due to differences in the physical losses over time as a function of particle size in the rotating drum chamber (P< 0.0001 for both parameters when compared using paired t-tests). The mean MMAD and GSD measured at the final sample for each test was 1.73 ± 0.13 μm and 1.60 ± 0.02, respectively (n = 74). Mean temperatures across all tests were within ±0.7 °C of the target value, and mean relative humidities across all tests were within ±2% of the target value.

Summary results of decay testing conducted across different combinations of environmental conditions are shown in Figures 4–6 and Table 1. In the absence of simulated sunlight, mean decay rates for infectious virus were less than 2% per minute for all temperature and humidity levels, except for 30 °C and 70% relative humidity, which had a mean decay rate of 6.3 ± 2.6% per minute, and 40 °C and 20% relative humidity, which has a mean decay rate of 3.9 ± 0.4% per minute (Figure 4). In the presence of high intensity simulated sunlight representative of noon at sea level on the summer solstice at 40°N latitude, mean decay rates ranged from a maximum of 38.1 ± 8.9% per minute at 40 °C and 20% relative humidity,

to 18.9 ± 4.8% per minute at 10 °C and 20% relative humidity (Figure 6). In the presence of lower intensity simulated sunlight, representative of fall or spring at 40°N latitude, mean decay rates ranged from 18.0 ± 6.2% per minute at 30 °C and 45% relative humidity, to 11.1 ± 4.6% per minute at 10 °C and 20% relative humidity (Figure 5).

Stepwise regression analysis performed with temperature, relative humidity, and simulated sunlight demonstrated that all three parameters, as well the interaction between temperature and simulated sunlight, were significant factors affecting $k_{infectivity}$. The overall adjusted r^2 for the model was 0.83, and the whole model ANOVA had a *p*-value of <0.0001. Decay rates predicted by this model were similar to the mean decay rates measured for each combination of environmental conditions (Table 1).

Stepwise regression analysis performed with absolute humidity, temperature, and simulated sunlight demonstrated that all three parameters, as well as the interaction between temperature and simulated sunlight, were significant factors affecting $k_{infectivity}$. The overall adjusted r^2 for the model was also 0.83, and the whole model ANOVA had a *p* value of <0.0001. The complete regression models using both relative and absolute humdity are shown in Equations (1) and (2), respectively. For both equations, the valid ranges for input paramters are 10 °C to 30 °C for temperature, and 0.0 W/m^2 to 1.9 W/m^2 for integrated UVB irradiance for spectra conforming to those used in the present study. The valid range for relative humidity in Equation (1) is 20% to 70%. For absolute humidity, the range of valid input values is dependent on the temperature, and can be found in Figures 4–6.

$$\begin{aligned} k_{infectivity} = {} & 0.16030 + 0.04018\left(\frac{(T - 20.615)}{10.585}\right) \\ & + 0.02176\left(\frac{(RH - 45.235)}{28.665}\right) \\ & + 0.14369\left(\frac{(S - 0.95)}{0.95}\right) \\ & + 0.02636\left(\frac{(T - 20.615)}{10.585}\right)\left(\frac{(S - 0.95)}{0.95}\right) \end{aligned} \tag{1}$$

where $k_{infectivity}$ = decay constant for viral infectivity, in min^{-1}, T = temperature, in °C, RH = relative humidity, in %, and S = integrated UVB irradiance, in W/m^2.

$$\begin{aligned} k_{infectivity} = {} & 0.17341 + 0.02218\left(\frac{(T - 20.615)}{10.585}\right) \\ & + 0.03955\left(\frac{(AH - 12.45)}{10.82}\right) \\ & + 0.14488\left(\frac{(S - 0.95)}{0.95}\right) \\ & + 0.02624\left(\frac{(T - 20.615)}{10.585}\right)\left(\frac{(S - 0.95)}{0.95}\right) \end{aligned} \tag{2}$$

where $k_{infectivity}$ = decay constant for viral infectivity, in min^{-1}, T = temperature, in °C, AH = absolute humidity, in g-H_2O/m^3-air, and S = integrated UVB irradiance, in W/m^2.

The standardized parameter estimates for each model are shown in Table 2. Comparison of the standardized coefficients for both models demonstrates that simulated sunlight had the greatest influence on $k_{infectivity}$ for the range of environmental conditions evaluated,

while relative/absolute humidity had the smallest influence. The model coefficients for temperature, simulated sunlight, and their interaction were similar regardless of whether relative or absolute humidity was used in the model.

Discussion

Previously, our laboratory reported that simulated sunlight, but not relative humidity, significantly increased the decay rate of infectious SARS-CoV-2 in aerosols at 20 °C (Schuit, Ratnesar-Shumate, et al. 2020). The present study expands upon these previous findings to include the influence of temperature, and is the first to report the influence of combinations of temperature, simulated sunlight, and humidity on the infectivity of SARS-CoV-2 in aerosols. While the results demonstrate that temperature, simulated sunlight, and humidity were all significant factors influencing the persistence of infectious of SARS-CoV-2 in aerosols, the magnitude of the effect of either simulated sunlight or temperature was much greater than that of humidity. For high intensity simulated sunlight representative of noon on a clear day on the summer solstice at sea level at 40°N latitude, the time needed for a 90% decrease in infectious virus ranged from 4.7 min at 40 °C and 20% relative humidity, to 10.9 min at 10 °C and 20% relative humidity. In the presence of lower intensity simulated sunlight representative of fall or spring at 40°N latitude, the time needed for a 90% decrease in infectious virus ranged from 11.5 min at 30 °C and 45% relative humidity, to 19.5 min for 10 °C and 45% relative humidity. In the absence of simulated sunlight, the virus was significantly more stable. The time needed for a 90% decrease in infectious virus ranged from 35 min at 30 °C and 70% relative humidity to 58 min at 40 °C and 20% relative humidity to greater than 2 h for all of the other conditions. Overall, these results suggest that the persistence of infectious SARS-CoV-2 in naturally occurring aerosols may be affected by environmental conditions, and that virus could remain infectious for extended periods of time under some environmental conditions, particularly indoor or nighttime conditions. These results are in agreement with several recently published studies which have suggested that environmental factors, including UV radiation, temperature, and humidity, may modulate the incidence of COVID-19 (Prata, Rodrigues, and Bermejo 2020; Rashed et al. 2020; Sehra et al. 2020). It is important to note, however, that while environmental conditions, in particular UV radiation, appear to significantly decrease the persistence SARS-CoV-2 in aerosols, it is unclear if the decay rates observed are large enough to influence the probability of transmission in outdoor environments. Other factors, in addition to the survival of virus in aerosols, have the potential to influence aerosol transmission of disease, and, therefore, also need to be considered in any assessment of the impact of environmental conditions on transmission. These factors include the size distribution and viral load of particles shed from the respiratory tract of infected individuals, the dose of infectious virus needed to cause disease via inhalation, and the proximity of individuals and airflow characteristics within a given space. Taken together, these data can be utilized to inform short range transport and dispersion modeling to better understand the impact of environmental conditions on risk associated with various disease transmission scenarios. Unfortunately, at the present time, data on the size distribution and viral load of respiratory particles shed from infected individuals and the infectious dose via inhalation have not been reported, limiting the ability to conduct such analyses.

As already noted, the infectivity of SARS-CoV-2 in aerosols was relatively stable in the absence of simulated sunlight, with decay rates of less than 2% per minute, or greater than approximately 2 h for a 90% loss of infectious virus, for the majority of temperature and humidity levels examined. These data are in agreement with previously published studies examining the persistence of SARS-CoV-2 (Fears et al. 2020; Smither et al. 2020; van Doremalen et al. 2020) and other coronaviruses (Ijaz et al. 1985) in aerosols. The results of the present study also demonstrate that increases in temperature increase the decay rate of infectious SARS-CoV-2 in aerosols. While the present study is the first to report this for SARS-CoV-2, this finding is consistent with previous studies examining the effect of temperature on the stability of coronavirus 229E and MERS-CoV in aerosols (Ijaz et al. 1985; Pyankov et al. 2018). This same trend was also observed for coronaviruses, including both SARS-CoV-2 and SARS-CoV-1, deposited on surfaces (Biryukov et al. 2020; Casanova et al. 2010; Chan et al. 2011).

Finally, the results of the present study suggest that humidity influences the decay rate of infectious SARS-CoV-2 in aerosols, although, as already noted, the magnitude of the effect of humidity observed in the present study was relatively small. At 20 °C, the decay rate ranged from 0.6 ± 0.6% per minute at 20% relative humidity to 1.5 ± 0.5% per minute at 70% relative humidity. These results are in agreement with several previously published studies. Smither et al. (2020) reported a difference of approximately 2% per minute between mid and high-level relative humidities for SARS-CoV-2 in aerosols at room temperature without UV present. Similarly, at 20 °C without UV present, Ijaz et al. (1985) reported a change in the half life from 67 ± 8 h at 50% relative humidity to either 26 ± 6 h at 30% relative humidity or 3.3 ± 0.2 h at 80% relative humidity. These differences are equivalent to a difference of less than 0.5% per minute between the highest and lowest decay rates, observed at 80% and 50% relative humidity, respectively. In our previous study, we reported that relative humidity did not significantly influence the decay rate of SARS-CoV-2 at 20 °C (Schuit, Ratnesar-Shumate, et al. 2020). It is possible that the expanded temperature range and increased number of tests performed in the present study relative to our previous study allowed detection of this small effect. The present study also performed regression analyses using absolute humidity. The results were nearly identical to those obtained with relative humidity, suggesting that the mean decay rate for a given set of environmental conditions can be predicted using either relative or absolute humidity.

While the results of the present study suggest that the survival of SARS-CoV-2 in naturally occurring aerosols may be influenced by environmental conditions, there are several limitations of the study. First, only a single particle size distribution with an MMAD of approximately 2 μm, representative of that expected to be produced during normal breathing or speaking, was investigated (Johnson and Morawska 2009). While SARS-CoV-2 is present in these particles, the vast majority of the particle mass is composed of other noninfectious, nonvolatile components present in the suspension medium, with the virus representing only a small fraction of the particle mass. Therefore, the persistence of larger particle sizes which are known to be generated during other respiratory events, such as coughing or speaking (Chao et al. 2009; Morawska et al. 2009), should be investigated as the greater mass of noninfectious material associated with these particles has the potential to shield virus present within a particle from environmental insults, increasing its persistence in the

environment (Dybwad and Skogan 2017; Kesavan et al. 2014; Lighthart and Shaffer 1997). Another limitation of the present study relates to the particle composition of generated aerosols. Aerosols were generated from concentrated virus diluted 1:10 into simulated saliva. Previous studies have demonstrated that the suspending medium can significantly affect the persistence of microorganisms (Dybwad and Skogan 2017). While the use of concentrated viral stocks was necessary to achieve quantifiable concentrations of infectious virus in the rotating drum chamber, the addition of the viral concentrate to the simulated saliva significantly changed both the protein content and fractional solids relative to the naïve simulated saliva. Therefore, additional testing is needed to confirm that the persistence data obtained for SARS-CoV-2 suspended in this matrix are representative of the persistence expected for SARS-CoV-2 in particles exhaled from infected individuals. Despite these limitations, the present study provides novel data that can be utilized, in conjunction with data on the viral load shed by infected individuals and the infectious dose in uninfected individuals, to inform modeling to better understand the impact of environmental conditions on risk associated with various disease transmission scenarios.

Funding

This work was funded under Agreement No. HSHQDC-15-C-00064 awarded to Battelle National Biodefense Institute by the Department of Homeland Security (DHS) Science and Technology Directorate (S&T) for the management and operation of the National Biodefense Analysis and Countermeasures Center (NBACC), a Federally Funded Research and Development Center. The views and conclusions contained in this document are those of the authors and should not be interpreted as necessarily representing the official policies, either expressed or implied, of DHS or the U.S. Government. The DHS does not endorse any products or commercial services mentioned in this presentation. In no event shall the DHS, BNBI or NBACC have any responsibility or liability for any use, misuse, inability to use, or reliance upon the information contained herein. In addition, no warranty of fitness for a particular purpose, merchantability, accuracy or adequacy is provided regarding the contents of this document.

References

Barreca AI, and Shimshack JP 2012. Absolute humidity, temperature, and influenza mortality: 30 years of county-level evidence from the United States. Am. J. Epidemiol176 Suppl 7:S114–S122. doi:10.1093/aje/kws259. [PubMed: 23035135]

Biryukov J, Boydston JA, Dunning RA, Yeager JJ, Wood S, Reese AL, Ferris A, Miller D, Weaver W, Zeitouni NE, et al. 2020. Increasing temperature and relative humidity accelerates inactivation of SARS-CoV-2 on surfaces. mSphere 5 (4):e00441. doi:10.1128/mSphere.00441-20. [PubMed: 32611701]

Casanova LM, Jeon S, Rutala WA, Weber DJ, and Sobsey MD 2010. Effects of air temperature and relative humidity on coronavirus survival on surfaces. Appl. Environ. Microbiol 76 (9):2712–7. doi:10.1128/AEM.02291-09. [PubMed: 20228108]

Chan KH, Peiris JS, Lam SY, Poon LL, Yuen KY, and Seto WH 2011. The effects of temperature and relative humidity on the viability of the SARS coronavirus. Adv. Virol 2011:734690. doi:10.1155/2011/734690. [PubMed: 22312351]

Chao C, Wan MP, Morawska L, Johnson GR, Ristovski ZD, Hargreaves M, Mengersen K, Corbett S, Li Y, Xie X, et al. 2009. Characterization of expiration air jets and droplet size distributions immediately at the mouth opening. J. Aerosol Sci 40 (2):122–33. doi:10.1016/j.jaerosci.2008.10.003. [PubMed: 32287373]

Chia PY, Coleman KK, Tan YK, Ong S, Gum M, Lau SK, Lim XF, Lim AS, Sutjipto S, Lee PH, et al. 2020. Detection of air and surface contamination by SARS-CoV-2 in hospital rooms of infected patients. Nat. Commun 11 (1):2800. doi:10.1038/s41467-020-16670-2. [PubMed: 32472043]

Darnell ME, Subbarao K, Feinstone SM, and Taylor DR 2004. Inactivation of the coronavirus that induces severe acute respiratory syndrome, SARS-CoV. J. Virol. Methods 121 (1):85–91. doi:10.1016/j.jviromet.2004.06.006. [PubMed: 15350737]

Docherty AB, Harrison EM, Green CA, Hardwick HE, Pius R, Norman L, Holden KA, Read JM, Dondelinger F, Carson G, et al. 2020. Features of 20 133 UK patients in hospital with covid-19 using the ISARIC WHO Clinical Characterisation Protocol: prospective observational cohort study. BMJ. 369. https://www.bmj.com/content/369/bmj.m1985

Dybwad M, and Skogan G. 2017. Aerobiological stabilities of different species of gram-negative bacteria, including well-known biothreat simulants, in single-cell particles and cell clusters of different compositions. Appl. Environ. Microbiol 83 (18):e00823. doi:10.1128/AEM.00823-17. [PubMed: 28687646]

Fears AC, Klimstra WB, Duprex P, Hartman A, Weaver SC, Plante KS, Mirchandani D, Plante JA, Aguilar PV, Fernández D, et al. 2020. Persistence of severe acute respiratory syndrome coronavirus 2 in aerosol suspensions. Emerg. Infect. Dis 26 (9):2168–71. doi:10.3201/eid2609.201806. [PubMed: 32568661]

Guo ZD, Wang ZY, Zhang SF, Li X, Li L, Li C, Cui Y, Fu RB, Dong YZ, Chi XY, et al. 2020. Aerosol and surface distribution of severe acute respiratory syndrome coronavirus 2 in hospital wards, Wuhan, China, 2020. Emerg. Infect. Dis 26 (7):1583–91. doi:10.3201/eid2607.200885. [PubMed: 32275497]

Ijaz MK, Brunner AH, Sattar SA, Nair RC, and Johnson-Lussenburg CM 1985. Survival characteristics of airborne human coronavirus 229E. J. General Virol 66 (12):2743–8. doi:10.1099/0022-1317-66-12-2743.

Johnson GR, and Morawska L. 2009. The mechanism of breath aerosol formation. J. Aerosol Med. Pulmonary Drug Del 22 (3):229–37. doi:10.1089/jamp.2008.0720.

Kesavan J, Schepers D, Bottiger J, and Edmonds J. 2014. UV-C decontamination of aerosolized and surface-bound single spores and bioclusters. Aerosol Sci. Tech 48 (4): 450–7. doi:10.1080/02786826.2014.889276.

Leung N, Chu D, Shiu E, Chan KH, McDevitt JJ, Hau B, Yen HL, Li Y, Ip D, Peiris J, et al. 2020. Respiratory virus shedding in exhaled breath and efficacy of face masks. Nat. Med 26 (5):676–80. doi:10.1038/s41591-020-0843-2. [PubMed: 32371934]

Lighthart B, and Shaffer BT 1997. Increased airborne bacterial survival as a function of particle content and size. Aerosol Sci. Tech 27 (3):439–46. doi:10.1080/02786829708965483.

Lindsley WG, Blachere FM, Thewlis RE, Vishnu A, Davis KA, Cao G, Palmer JE, Clark KE, Fisher MA, Khakoo R, et al. 2010. Measurements of airborne influenza virus in aerosol particles from human coughs. PloS One 5 (11):e15100. doi:10.1371/journal.pone.0015100. [PubMed: 21152051]

Liu Y, Ning Z, Chen Y, Guo M, Liu Y, Gali NK, Sun L, Duan Y, Cai J, Westerdahl D, et al. 2020. Aerodynamic analysis of SARS-CoV-2 in two Wuhan hospitals. Nature 582 (7813):557–60. doi:10.1038/s41586020-2271-3. [PubMed: 32340022]

Lovato A, and de Filippis C. 2020. Clinical presentation of COVID-19: A systematic review focusing on upper airway symptoms. Ear Nose Throat J. 99 (9): 569–576. doi: 10.1177/0145561320920762. [PubMed: 32283980]

McDevitt J, Rudnick S, First M, and Spengler J. 2010. Role of absolute humidity in the inactivation of influenza viruses on stainless steel surfaces at elevated temperatures. Appl. Environ. Microbiol 76 (12):3943–7. doi:10.1128/AEM.02674-09. [PubMed: 20435770]

Morawska L, Johnson GR, Ristovski ZD, Hargreaves M, Mengersen K, Corbett S, Chao CYH, Li Y, and Katoshevski D. 2009. Size distribution and sites of origin of droplets expelled from the human respiratory tract during expiratory activities. J. Aerosol Sci 40 (3): 256–69. doi:10.1016/j.jaerosci.2008.11.002.

National Center for Atmospheric Research. 2020. Tropospheric ultraviolet and visible (TUV) radiation model. Accessed on 28 Jun 2020. https://www2.acom.ucar.edu/modeling/tropospheric-ultraviolet-and-visible-tuv-radiation-model.

Prata DN, Rodrigues W, and Bermejo PH 2020. Temperature significantly changes COVID-19 transmission in (sub)tropical cities of Brazil. Sci. Total Environ 729:138862. doi:10.1016/j.scitotenv.2020.138862. [PubMed: 32361443]

Pyankov OV, Bodnev SA, Pyankova OG, and Agranovski IE 2018. Survival of aerosolized coronavirus in the ambient air. J. Aerosol Sci 115:158–63. doi:10.1016/j.jaerosci.2017.09.009. [PubMed: 32226116]

Rashed EA, Kodera S, Gomez-Tames J, and Hirata A. 2020. Influence of absolute humidity, temperature and population density on COVID-19 Spread and Decay Durations: Multi-Prefecture Study in Japan. IJERPH 17 (15):5354. doi:10.3390/ijerph17155354. [PubMed: 32722294]

Ratnesar-Shumate S, Williams G, Green B, Krause M, Holland B, Wood S, Bohannon J, Boydston J, Freeburger D, Hooper I, et al. 2020. Simulated sunlight rapidly inactivates SARS-CoV-2 on surfaces. J. Infect Dis 222 (2):214–22. doi:10.1093/infdis/jiaa274. [PubMed: 32432672]

Schuit M, Gardner S, Wood S, Bower K, Williams G, Freeburger D, and Dabisch P. 2020. The influence of simulated sunlight on the inactivation of influenza virus in aerosols. J. Infect. Dis 221 (3):372–8. doi:10.1093/infdis/jiz582. [PubMed: 31778532]

Schuit M, Ratnesar-Shumate S, Yolitz J, Williams G, Weaver W, Green B, Miller D, Krause M, Beck K, Wood S, et al. 2020. Airborne SARS-CoV-2 Is rapidly inactivated by simulated sunlight. J. Infect. Dis 222 (4): 564–71. doi:10.1093/infdis/jiaa334. [PubMed: 32525979]

Sehra ST, Salciccioli JD, Wiebe DJ, Fundin S, and Baker JF 2020. maximum daily temperature, precipitation, ultra-violet light and rates of transmission of SARS-Cov-2 in the United States. Clin. Infect. Dis. Off. Publ. Infect. Dis. Soc. Am doi:10.1093/cid/ciaa681.

Shaman J, Goldstein E, and Lipsitch M. 2011. Absolute humidity and pandemic versus epidemic influenza. Am. J. Epidemiol 173 (2):127–35. doi:10.1093/aje/kwq347. [PubMed: 21081646]

Smither SJ, Eastaugh LS, Findlay JS, and Lever MS 2020. Experimental aerosol survival of SARS-CoV-2 in artificial saliva and tissue culture media at medium and high humidity. Emerg. Microbes Infect 9 (1):1415–7. doi: 10.1080/22221751.2020.1777906. [PubMed: 32496967]

van Doremalen N, Bushmaker T, Morris DH, Holbrook MG, Gamble A, Williamson BN, Tamin A, Harcourt JL, Thornburg NJ, Gerber SI, et al. 2020. Aerosol and Surface Stability of SARS-CoV-2 as Compared with SARS-CoV-1. New Engl. J. Med 382 (16):1564–7. doi:10.1056/NEJMc2004973. [PubMed: 32182409]

Yang W, Elankumaran S, and Marr LC 2011. Concentrations and size distributions of airborne influenza A viruses measured indoors at a health centre, a day-care centre and on aeroplanes. J. R. Soc. Interface 8 (61):1176–84. doi:10.1098/rsif.2010.0686. [PubMed: 21300628]

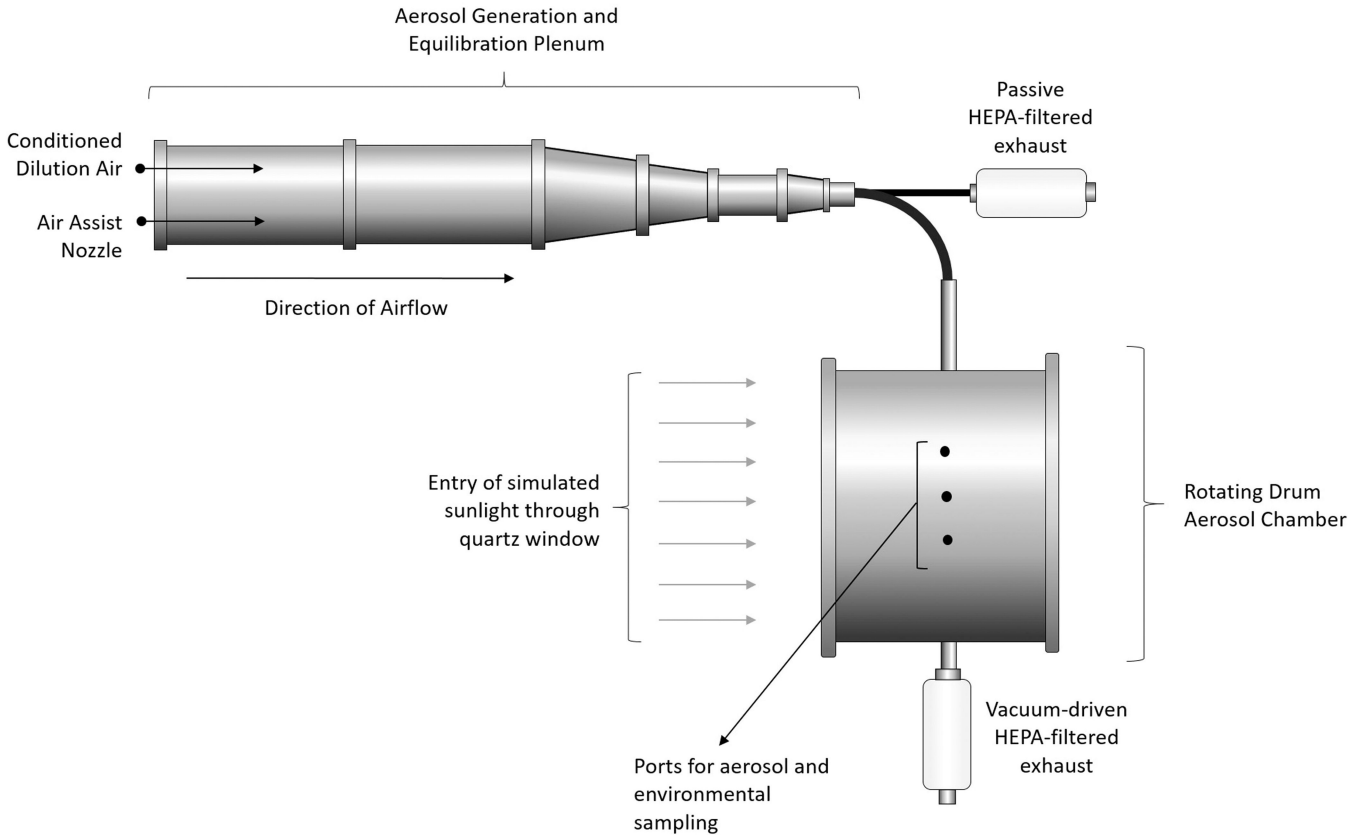

Figure 1.

Schematic of rotating drum aerosol chamber. A 16-L environmentally controlled rotating drum aerosol chamber was used to assess the effect of environmental parameters on the decay rate of SARS-CoV-2. The temperature of the air inside the chamber was controlled by adjusting the temperature of polypropylene glycol circulating through the walls of the chamber. The humidity inside the chamber was controlled by varying the mix of dry and humid air used to supply the chamber during aerosol filling and sampling. Simulated sunlight was introduced into the chamber through a quartz glass window located on one end of the chamber, as indicated by the arrows in the figure. Aerosols with a target MMAD of 2 μm were generated with an air assist nozzle into a humidity controlled stainless steel plenum that was exhausted through a HEPA filter. A portion of this flow was diverted into the rotating drum for 20–30 s during filling to achieve a quantifiable concentration of infectious virus. Multiple samples were collected over the duration of the test to estimate infectious viral concentrations and total aerosol mass concentrations over time from sampling ports located on a non-rotating band in the wall of the rotating drum.

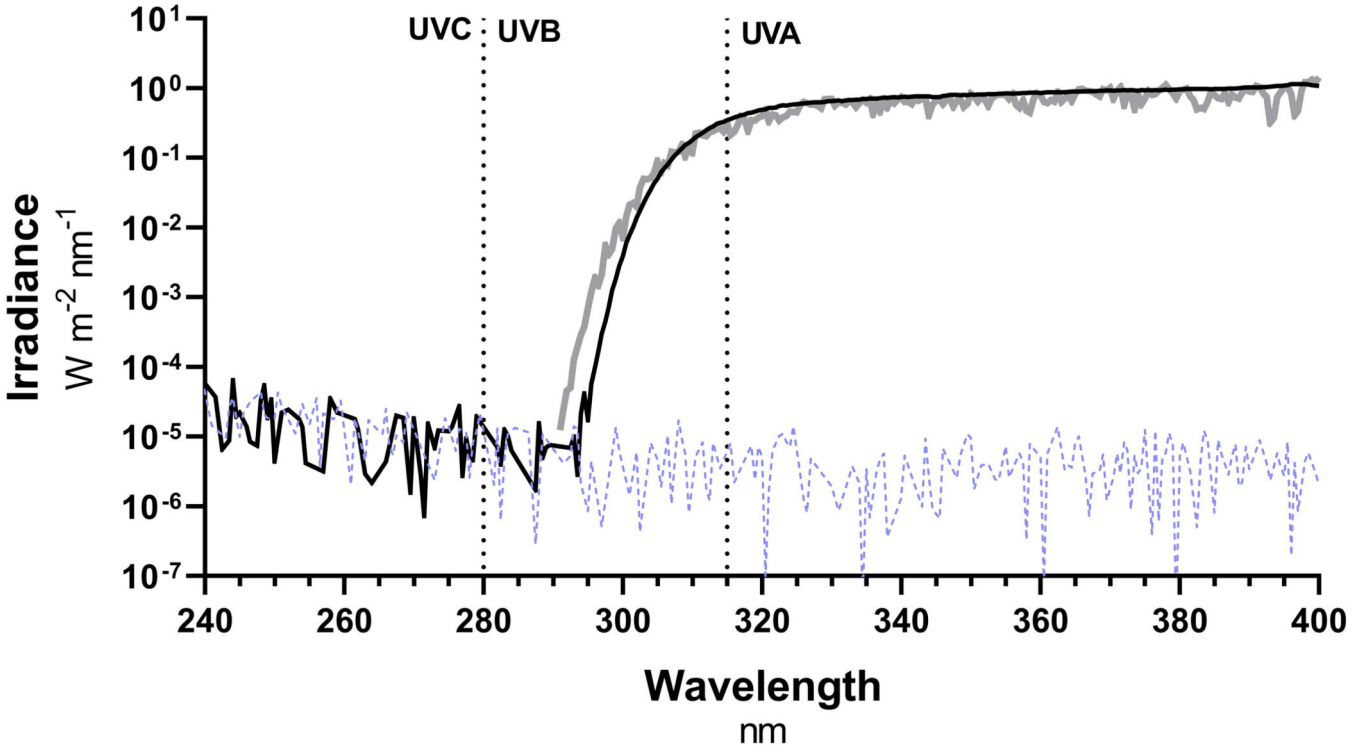

Figure 2.

Comparison of simulated sunlight UV spectrum to NCAR TUV model spectrum. The spectrum generated by the solar simulator (black) was similar to that predicted by NCAR's TUV radiation model for 40°N latitude on 21 June at noon at sea level under cloudless conditions (gray). Integrated UVB irradiances were 1.91 W/m^2 and 1.84 W/m^2 for the solar simulator and TUV radiation model, respectively. No irradiance above the background level of the spectroradiometer measured in darkness (dashed line) was present in the spectrum generated by the solar simulator below approximately 295 nm.

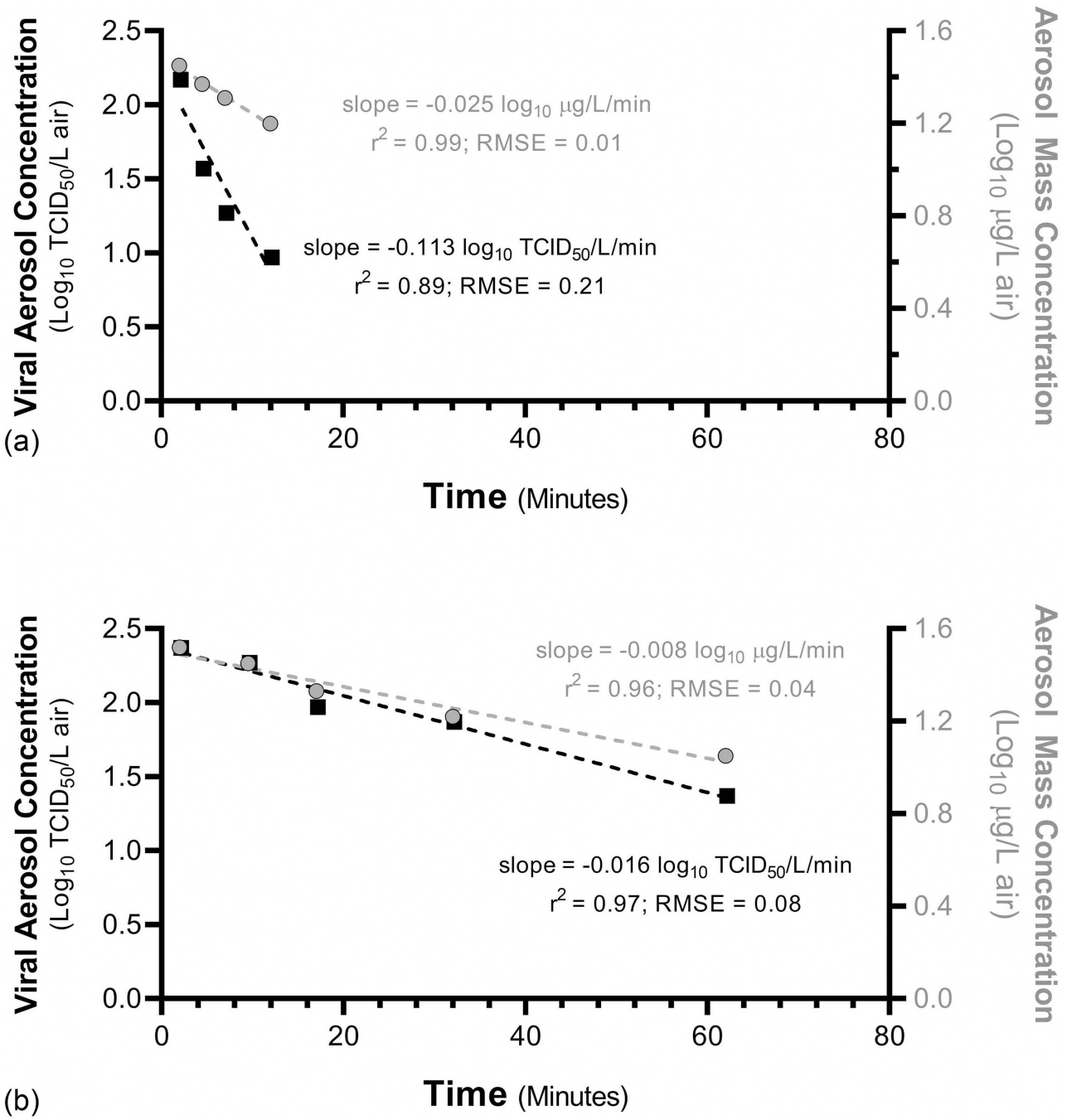

Figure 3.

Representative decay plots. The slopes of the best fit lines for time-series $\log_{10}$-transformed infectious and mass aerosol concentrations from each test were used as estimates of the total and physical decays, respectively. Total decay rates calculated from filter samples were normalized for physical losses by subtracting the physical decay rate calculated from APS samples to estimate the decay rate for viral infectivity. Decay plots from tests at (a) 30 °C, 1.9 W/m^2 integrated UVB, and 20% relative humidity and (b) 10 °C, 0.0 W/m^2 integrated UVB, and 70% relative humidity are shown. The decay rate for viral infectivity is greater for

(a) 30 °C, 1.9 W/m^2 integrated UVB, and 20% relative humidity relative to (b) 10 °C, 0.0 W/m^2 integrated UVB, and 70% relative humidity, as can be seen from the larger difference between the slopes of viral (black) and mass (gray) aerosol concentrations.

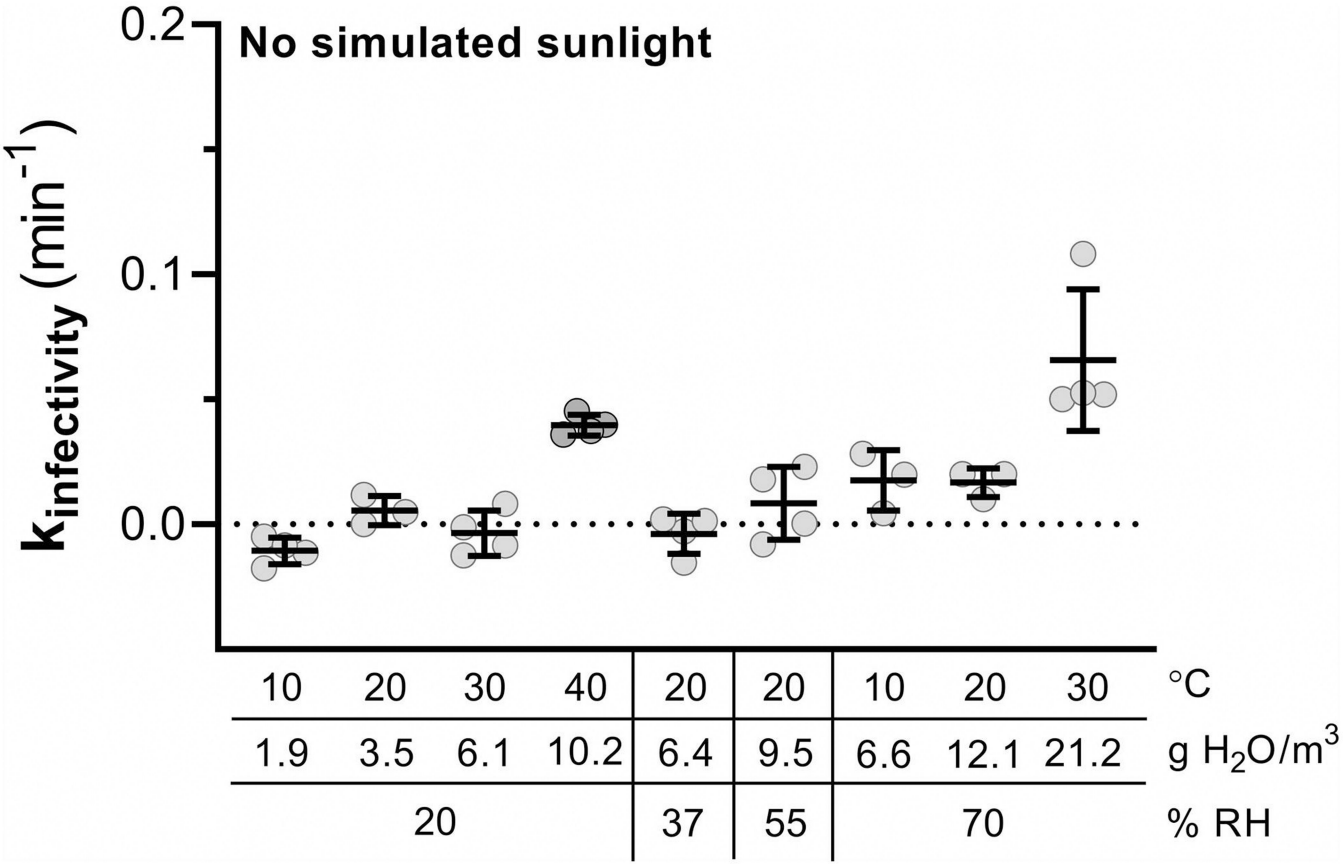

Figure 4.

Decay constants for viral infectivity as a function of temperature and humidity without simulated sunlight. Both relative and absolute humidity levels are shown on the x-axis, along with temperature. Decay constants were near zero for most conditions, but increased at both 40 °C/20% relative humidity and 30 °C/70% relative humidity. Lines indicate arithmetic mean ± one standard deviation.

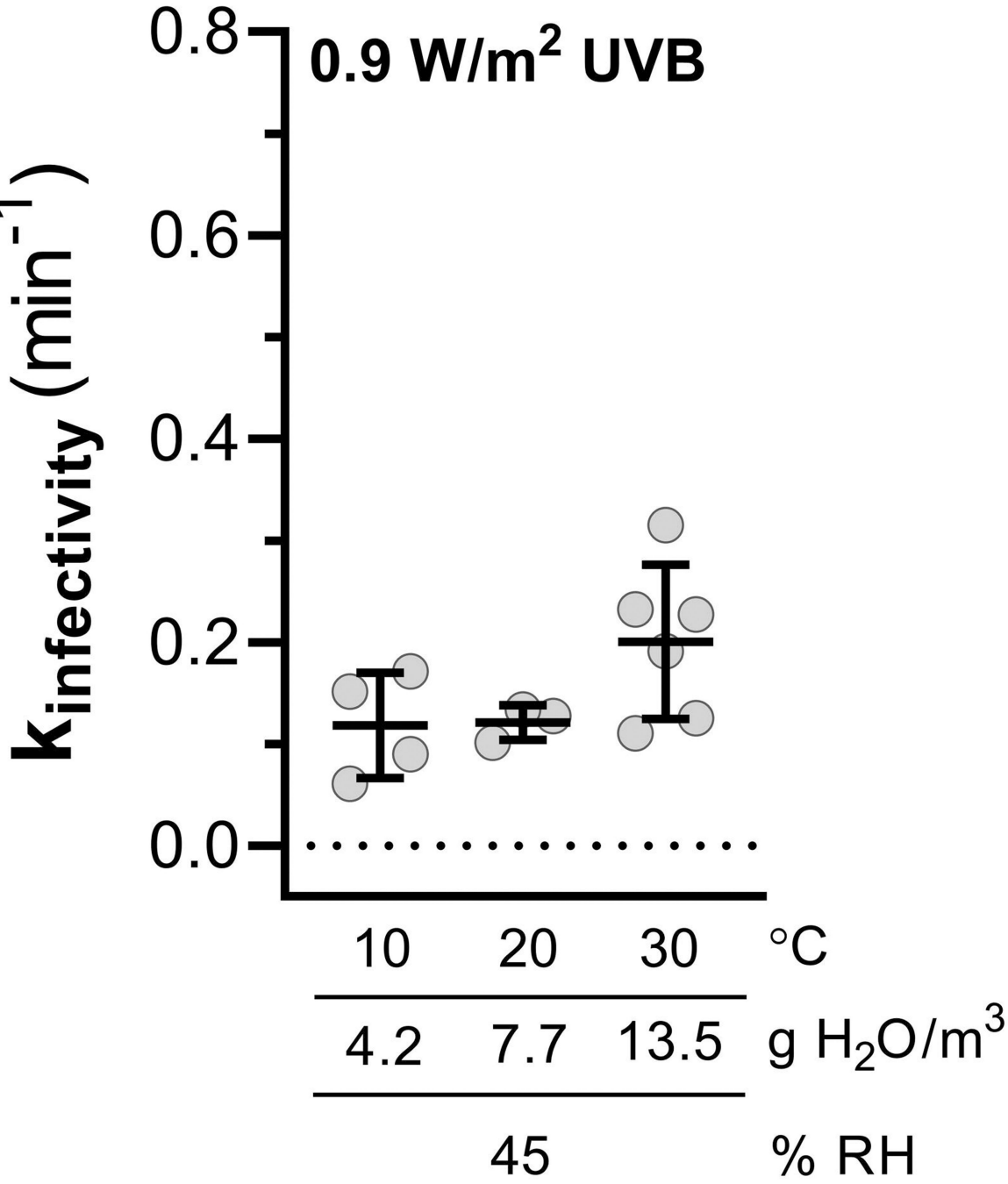

Figure 5.

Decay constants for viral infectivity as a function of temperature and humidity at 0.9 W/m^2 UVB irradiance. Both relative and absolute humidity levels are shown on the x-axis, along with temperature. Lines indicate arithmetic mean ± one standard deviation. Data at 20 °C and 45% relative humidity are from Schuit, Ratnesar-Shumate, et al. (2020).

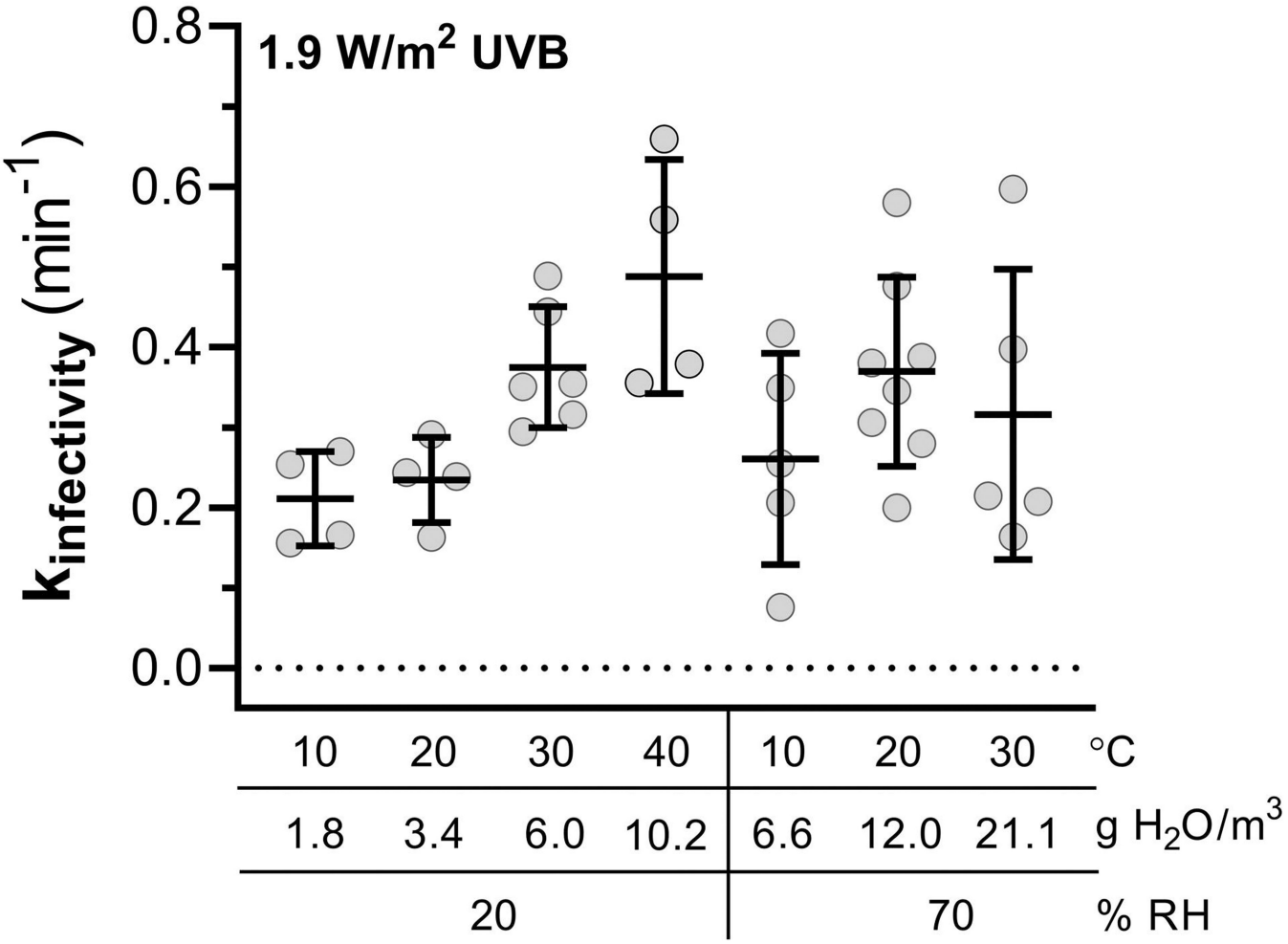

Figure 6.

Decay constants for viral infectivity as a function of temperature and humidity at 1.9 W/m^2 UVB irradiance. Both relative and absolute humidity levels are shown on the x-axis, along with temperature. Lines indicate arithmetic mean ± one standard deviation. Data at 20 °C and 20% relative humidity are from Schuit, Ratnesar-Shumate, et al. (2020). The variability associated with measurement of $k_{infectivity}$ was significantly increased relative to measurements at lower simulated sunlight levels, especially at higher relative humidities.

Table 1.

Decay as function of environmental conditions. Mean decay constants and decay rates are shown for each combination of environmental conditions evaluated. Values are presented as arithmetic mean ± one standard deviation. *Denotes data reported in Schuit, Ratnesar-Shumate, et al. (2020).

Integrated UVB Irradiance (W/m^2)	Temp (°C)	Relative Humidity (%)	Absolute Humidity (g-H_2O/m^3-air)	$k_{infectivity}$ (min^{-1})	Decay Rate (% loss /min)	Predicted Decay Rate from RH Model (% loss /min)	n
0	10	20	1.8	−0.011 ± 0.005	−1.0 ± 0.5	−1.7	4
		70	6.6	0.018 ± 0.012	1.7 ± 1.2	2.1	3
	20	20	3.4	0.006 ± 0.006	0.6 ± 0.6	− 0.3	3
		70	12.0	0.017 ± 0.006	1.5 ± 0.5	3.4	3
	30	20	6.0	− 0.003 ± 0.009	− 0.4 ± 0.9	1.0	4
		70	21.1	0.066 ± 0.028	6.3 ± 2.6	4.7	4
	40	20	10.2	0.040 ± 0.004	3.9 ± 0.4	2.3	4
0.9	10	45	4.2	0.118 ± 0.052	11.1 ± 4.6	10.7	4
	20	45	7.7	0.121 ± 0.017*	11.4 ± 1.5*	14.0	3
	30	45	13.5	0.200 ± 0.076	18.0 ± 6.2	17.1	6
1.9	10	20	1.8	0.211 ± 0.059	18.9 ± 4.8	19.6	4
		70	6.6	0.261 ± 0.132	22.4 ± 10.4	22.6	5
	20	20	3.4	0.234 ± 0.053*	20.8 ± 4.2*	24.5	4
		70	12.0	0.369 ± 0.118	30.5 ± 7.9	27.3	8
	30	20	6.0	0.375 ± 0.076	31.1 ± 5.1	29.1	6
		70	21.1	0.316 ± 0.181	26.2 ± 12.5	31.7	5
	40	20	10.2	0.488 ± 0.146	38.1 ± 8.9	33.4	4

Table 2.

Standardized Coefficients for Regression Analyses Peformed with Relative Humidity or Absolute Humidity. Comparison of the standardized coefficients allow the magnitude of the effect of each parameter to be directly compared. For the range of environmental conditions tested, sunlight had the greatest influence on the decay constant for infectivity in either model, followed by temperature and their interaction. Humidity, regardless of whether it was expressed as relative or absolute humidity, had the smallest influence on the decay constant for infectivity. Best fit values are presented with 95% confidence intervals for each coefficient in parentheses underneath.

	Standardized Regression Coefficients	
Environmental Parameter	**Model with Relative Humidity**	**Model with Absolute Humidity**
Temperature (C)	0.04018 (0.1788 to 0.06247)	0.02218 (−0.00154 to 0.04589)
Simulated Sunlight (W/m^2 UVB)	0.14369 (0.12620 to 0.16118)	0.14488 (0.12771 to 0.16205)
Relative Humidity (%)	0.02176 (0.00980 to 0.03372)	NA
Absolute Humidity ($g\text{-}H_2O/m^3$-air)	NA	0.03955 (0.01973 to 0.05937)
Temperature (°C) × Solar (W/m^2 UVB)	0.02636 (0.00292 to 0.04981)	0.02624 (0.00321 to 0.04926)